ResearchGate

See discussions, stats, and author profiles for this publication at:
https://www.researchgate.net/publication/223620364

Structure and properties of the weakly bound trimer (H2O)2HCl. Theoretical predictions and comparison with high-resolution rotational spectroscopy

ARTICLE *in* CHEMICAL PHYSICS · SEPTEMBER 2001

Impact Factor: 1.65 · DOI: 10.1016/S0301-0104(01)00449-9

CITATIONS
18

READS
23

7 AUTHORS, INCLUDING:

Joanna Sadlej
University of Warsaw
275 PUBLICATIONS **8,645** CITATIONS

SEE PROFILE

Available from: Joanna Sadlej
Retrieved on: 26 January 2016

ELSEVIER

Chemical Physics 271 (2001) 267–282

Chemical Physics

www.elsevier.com/locate/chemphys

Structure and properties of the weakly bound trimer $(H_2O)_2HCl$. Theoretical predictions and comparison with high-resolution rotational spectroscopy

A. Milet [a,b], C. Struniewicz [b], R. Moszynski [b,c,*], J. Sadlej [b], Z. Kisiel [d], E. Białkowska-Jaworska [d], L. Pszczółkowski [d]

[a] *Laboratoire d'Etudes Dynamiques et Structurales de la Sélectivité, UMR 5616, LEDSS VII Chimie Théorique, Université Joseph Fourier, D.U. BP 53, 38041 Grenoble Cedex 9, France*

[b] *Department of Chemistry, University of Warsaw, Pasteura 1, 02-093 Warsaw, Poland*

[c] *Laboratoire de Chimie Théorique, UMR 7551 CNRS/ULP, Institut Le Bel, Université Louis Pasteur, 4, rue Blaise Pascal, F-67008 Strasbourg, France*

[d] *Institute of Physics, Polish Academy of Sciences, Al. Lotników 32/46, 02-668 Warsaw, Poland*

Received 28 March 2001; in final form 4 July 2001

Abstract

In this paper we report ab initio predictions of the minimum energy structure of the $(H_2O)_2HCl$ cluster, its stationary points, low-energy tunneling pathways, the dipole moment, and the nuclear quadrupole coupling constants. Structures corresponding to the stationary points were optimized with the second-order Møller–Plesset theory, while the corresponding interaction energies and binding energies were computed using the coupled-cluster method restricted to single, double, and non-iterative triple excitations. It is shown that the non-additive interactions play an important role. The contribution of the three-body term represents as much as 13–20% of the total interaction energy. The nature of the intermolecular interactions in the cluster was investigated by symmetry-adapted perturbation theory. As expected, the complex is mostly stabilized by the electrostatic and induction interactions, but the dispersion term is far from negligible. It is found that the potential energy surface of this cluster shows three low-energy pathways connecting two enantiomeric minimum energy structures. The height of the barriers separating these minima suggests that it should be possible to observe spectroscopic transitions resulting from the tunneling between the equivalent minima. From the study of these low-energy rearrangement processes we determined the permutation-inversion group of the complex, classified its vibration–rotation–tunneling states, and determined the electric dipole selection rules and spin-statistical weights governing the intensity pattern in the spectra. The results of the theoretical predictions are compared with the experimental data from the microwave measurements [Z. Kisiel et al., J. Chem. Phys. 112 (2000) 5767; Chem. Phys. Lett. 325 (2000) 523]. © 2001 Elsevier Science B.V. All rights reserved.

1. Introduction

Molecular complexes are the subject of continuing investigations in the fields of atmospheric chemistry, catalytic reactions, surface chemistry,

* Corresponding author. Address: Department of Chemistry, University of Warsaw, Pasteura 1, 02-093 Warsaw, Poland.
E-mail address: rmoszyns@chem.uw.edu.pl (R. Moszynski).

0301-0104/01/$ - see front matter © 2001 Elsevier Science B.V. All rights reserved.
PII: S0301-0104(01)00449-9

and biological processes. The answers to questions of how molecules select one of several competing reaction channels or of how they are oriented at surfaces and in clusters are all associated with the understanding of small energetic differences on the potential surfaces endowed with many local minima. A considerable amount of detailed experimental information on intermolecular complexes has recently become available from high-resolution spectroscopic studies [1,2]. However, for complexes with rich internal dynamics the otherwise very successful spectroscopic techniques often have difficulty in unambiguously determining the equilibrium molecular geometry and the details of the potential energy surface. A complementary route in this direction is offered by ab initio calculations. The advances in the computational techniques and in the computer power have turned this method into an accepted tool for the study of the structure, properties, and potential energy surfaces for the molecular complexes [3,4]. This fact was demonstrated in several seminal works of Del Bene and collaborators [5–7], especially for hydrogen-bonded complexes showing strong anharmonicities in the infrared spectra [5,6], and very unusual spin–spin coupling constants across the hydrogen bond [7].

The study of the interaction between water and hydrogen chloride is of fundamental importance for the understanding of strong aqueous acids. It is also of relevance to atmospheric chemistry since the $(H_2O)_nHCl$ clusters are implicated in the production of stratospheric Cl_2 molecules which, in turn, take part in the catalytic ozone depletion reactions. The mainly heterogeneous atmospheric reaction beginning with the adsorption of the HCl molecules on the surface of water icicles is the source of the stratospheric chlorine atoms in the polar regions [8–10]. Chlorine molecules are photolyzed by solar radiation and the resultant chlorine atoms take part in the destruction of the stratospheric ozone. The study of the $(H_2O)_nHCl$ clusters is an important step towards understanding of the behavior of the HCl molecule on the ice surface.

One route to understanding solvation of HCl has been through molecular dynamics studies of the $(H_2O)_nHCl$ clusters [11–13]. This method simulates proton transfer and/or the dissociation process in an aqueous solution, and the goal has been to determine the number of water molecules which are needed to cause ionic solvation of the HCl molecule. The recent simulation [11,13] of HCl with a solid water cluster showed that the ionic dissociation can take place on the surface of ice crystals.

An alternative method of investigating the solvation of HCl has been through the study of the isolated $(H_2O)_nHCl$ clusters of increasing size [14–20] in order to follow the increasing role of the cooperative effects and to establish the size threshold for the onset of ionization. Packer and Clary [20] reported ab initio calculations for $(H_2O)_nHCl$, $n = 1$–3, and have identified the cooperative effects of the hydrogen bonding in the trimer. The $(H_2O)_nHCl$, $n = 1$–5, clusters were also studied with the density functional and MP2 methods [17–19]. It was found that the proton transfer from HCl to the water molecule occurs in the case of the pentamer. Although global minima for these species have generally been identified, finer details of the energetics remain unknown. Spectroscopic properties of these clusters are expected to be dominated by their rich internal dynamics and this problem has not yet been touched upon. The same applies to the values of many observables pertinent to the spectroscopic methods with which the higher members of series might be expected to be observed.

Only the first members of the $(H_2O)_nHCl$ series have been observed by means of high resolution spectroscopy. The dimer $H_2O\cdots HCl$ has been first observed by Legon and Willoughby [21], and recently reinvestigated in Ref. [22]. In two recent papers [23,24] we reported the observation by rotational spectroscopy of the second member of the series: $(H_2O)_2HCl$. The purpose of this paper is to present a comprehensive study of the structure and dynamics of this trimer in order to lay the groundwork for the interpretation of the present and of the future experimental results. In the longer term we aim to provide insight into the microsolvation of HCl at the molecular level via a thorough investigation of the energetics, structures, properties, and interactions also for the higher members of the series [25,26].

2. Methods of calculations

In the present paper we investigated the lowest energy structures of the $(H_2O)_2HCl$ complex and the saddle points connecting various minima on the potential energy surface. The optimal geometries corresponding to these structures were obtained from analytic gradient calculations with the second-order Møller–Plesset theory (MP2). We performed full geometry optimization, i.e. the geometrical parameters of water and HCl were not fixed at their equilibrium values. In addition, harmonic frequency calculations at the same level of the theory were performed in order to check whether the stationary points obtained from the gradient calculations correspond to minima (all frequencies real) or saddle points (one imaginary frequency). The geometry optimization and frequency calculations were carried out with the GAUSSIAN98 code [27]. In all calculations we used the aug-cc-pVDZ basis set [28,29]. As shown in Refs. [30–32] this basis set reproduces rather well the geometries, frequencies, and electric properties of various hydrogen-bonded clusters. For the lowest energy structures we also computed the total interaction energy and the electronic binding and dissociation energies (denoted by D_e and D_0, respectively). The interaction energy was computed within the supermolecule approach by using the coupled-cluster method including single, double, and non-iterative triple excitations (CCSD(T)). The CCSD(T) interaction energy was represented by the following many-body expansion:

$$E_{\mathrm{int}}^{\mathrm{CCSD(T)}} = E_{\mathrm{int}}^{\mathrm{CCSD(T)}}(2,3) + E_{\mathrm{int}}^{\mathrm{CCSD(T)}}(3,3), \tag{1}$$

where in general $E_{\mathrm{int}}^{\mathrm{CCSD(T)}}(N,3)$ denotes the N-body contribution ($N \leqslant 3$) to the supermolecule interaction energy for a cluster of three molecules. The pair and three-body interaction energies are given by the standard formulas,

$$E_{\mathrm{int}}^{\mathrm{CCSD(T)}}(2,3) = \frac{1}{2}\sum_{i\neq j=1}^{3}\left(E_{X_iX_j}^{\mathrm{CCSD(T)}} - E_{X_i}^{\mathrm{CCSD(T)}} - E_{X_j}^{\mathrm{CCSD(T)}}\right), \tag{2}$$

$$E_{\mathrm{int}}^{\mathrm{CCSD(T)}}(3,3) = E_{X_1X_2X_3}^{\mathrm{CCSD(T)}} - E_{X_1X_2}^{\mathrm{CCSD(T)}} - E_{X_2X_3}^{\mathrm{CCSD(T)}} - E_{X_3X_1}^{\mathrm{CCSD(T)}} + E_{X_1}^{\mathrm{CCSD(T)}} + E_{X_2}^{\mathrm{CCSD(T)}} + E_{X_3}^{\mathrm{CCSD(T)}}, \tag{3}$$

where $E_{X_1\cdots X_m}^{\mathrm{CCSD(T)}}$ denotes the total energy of a system composed of molecules $X_1,\ldots,X_m$. The supermolecular energy was corrected for the basis-set superposition error (BSSE) with the counterpoise method of Boys and Bernardi [33] by performing the calculation of the interaction energy in the full basis of the trimer. The binding energy D_e was obtained from the interaction energy by correcting the latter for the deformation energy E_{def} [34], i.e. for the energy needed to deform the monomers from their optimal equilibrium geometries to their geometries in the complex. The latter quantity was computed in the bases of the respective monomers. Finally, the dissociation energy D_0 was obtained from the binding energy by adding the correction for the zero-point vibrational motion. In our work, the zero-point correction was calculated at the MP2 level in the harmonic approximation. In the supermolecule CCSD(T) calculations we employed the GAUSSIAN98 code and kept the 1s orbitals frozen.

In order to get an insight into the origins of the bonding in the $(H_2O)_2HCl$ cluster we performed additional calculations of the pair interaction energies by symmetry-adapted perturbation theory (SAPT) [3]. The SAPT calculations of the non-additive three-body energies are feasible at present [35–40], and the three-body effects in the $(H_2O)_2$-HCl trimer are considered in Ref. [41]. Thus, in the present work we will characterize the nature of the interactions in the trimer in the pair approximation. The pair interaction energy was computed from the following expression:

$$E_{\mathrm{int}}^{\mathrm{SAPT}}(2,3) = E_{\mathrm{elst}}^{(1)} + E_{\mathrm{ind}}^{(2)} + E_{\mathrm{disp}}^{(2)} + E_{\mathrm{exch}}, \tag{4}$$

where the consecutive terms on the right-hand side of Eq. (4) denote the electrostatic, induction, dispersion, and exchange energies, respectively. The exchange contribution can further be decomposed as follows:

$$E_{\mathrm{exch}} = E_{\mathrm{exch}}^{(1)} + E_{\mathrm{exch\text{-}ind}}^{(2)} + E_{\mathrm{exch\text{-}def}}^{(2)} + E_{\mathrm{exch\text{-}disp}}^{(2)}. \tag{5}$$

Here, $E^{(1)}_{\text{exch}}$ is the first-order exchange energy, while $E^{(2)}_{\text{exch-ind}}$, $E^{(2)}_{\text{exch-def}}$, and $E^{(2)}_{\text{exch-disp}}$ denote the exchange-induction, exchange-deformation, and exchange-dispersion terms. The contributions appearing on the right-hand side of Eqs. (4) and (5) have been evaluated using the many-body techniques developed in Refs. [42–50]. The exchange-deformation energy was computed directly from the supermolecule Hartree–Fock interaction energy. The computational scheme for the pair interactions was the same as in our previous works (see, for instance, Ref. [51]). The SAPT calculations of the pair interaction energies were made with the program SAPT [52]. The SAPT pair energies were always computed with dimer basis sets.

Finally, we also considered the electric properties of the $(H_2O)_2HCl$ trimer. The dipole moment and nuclear quadrupole coupling constants at the MP2 level were calculated as analytical derivatives of the corresponding energies. The CCSD(T) dipole moment was obtained by using the finite field technique (the field strength was set equal to 0.001 a.u.).

3. Theoretical predictions

3.1. Global minimum and low-energy tunneling pathways

The global minimum on the potential energy surface of the $(H_2O)_2HCl$ trimer corresponds to a cyclic triangular hydrogen-bonded structure (see Fig. 1) with both HCl and the two water monomers acting simultaneously as proton donors and acceptors. Due to geometrical constraints the hydrogen bonds are rather strongly bent. The hydrogen atoms not involved in the hydrogen bonds lie alternatively above and below the plane of the hydrogen-bonded ring (denoted 'up' and 'down', or *u* and *d*). This structure has no spatial symmetry, but there are two equivalent minima corresponding to the up–down (or *ud*) and down–up (*du*) enantiomeric structures. The distances between the oxygen and chlorine atoms in the trimer are 3.02 and 3.39 Å for $r(O_ACl)$ and $r(O_BCl)$, respectively. The former is slightly smaller than the

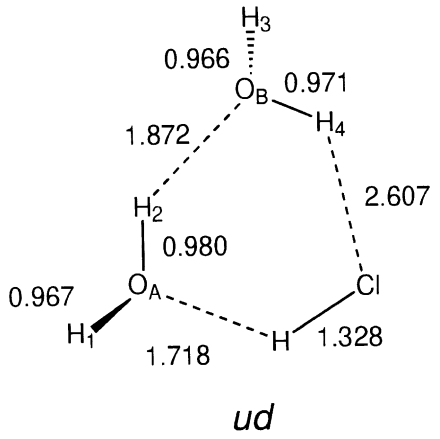

Fig. 1. Geometry of the global (*ud*) minimum on the potential energy surface of the $(H_2O)_2HCl$ trimer.

$O\cdots Cl$ distance in the $H_2O\cdots HCl$ dimer, 3.09 Å [14], while the latter is somewhat larger. (The numbering of the atoms is the same as in Fig. 1.) The $O\cdots O$ distance is 2.79 Å and is also smaller than the corresponding distance in the water dimer, 2.91 Å. This shortening of the distances between the heavy atoms in the trimer in comparison with the distances in the respective dimers imposes rather strong strains in the hydrogen bonds. The heavy atoms (oxygens and chlorine) form a deformed equilateral triangle, with the angles $\angle ClO_AO_B$ and $\angle ClO_BO_A$ being equal to 71.1° and 57.7°, respectively. The hydrogen atoms forming hydrogen bonds lie almost perfectly in the plane of the heavy atoms (the dihedral angles between the respective planes being smaller than 3°), while the external protons H_1 and H_3 are distorted from the hydrogen-bonded ring by about 122° and 134°, respectively. The full set of Cartesian coordinates defining the equilibrium geometry of $(H_2O)_2HCl$ is reported in Table VII of Ref. [23]. One may note here that the equilibrium structure of the $(H_2O)_2HCl$ trimer is quite similar to the structure of the water trimer [53]. The $O\cdots O$ distances are very close (2.79 Å in the former vs. 2.80 Å in the latter), while the distances between the oxygen atoms and the chlorine atom in $(H_2O)_2HCl$ do not differ much from the $O\cdots O$ distance in the water trimer (3.02 and 3.38 Å, respectively, vs. 2.80 Å). To continue this paragraph let us mention that the

lowest energy structure of the $(H_2O)_2HCl$ trimer was previously considered in Refs. [15–17,20]. Our results agree very well with the previous calculations and differ by 0.002 Å for the distances, 0.1° for the angles, and 1° for the dihedral angles (we give the largest deviations from the set of the previous calculations cited above). As shown in Ref. [23] the theoretical equilibrium structure is in a very good agreement with the structure derived from the microwave measurements.

To connect the structures corresponding to the equivalent global minima, we considered three low-energy pathways. Schematic representations of these pathways are reported in Figs. 2, 3(a) and (b). Although in principle other paths could be considered, we have checked that they are much higher in energy. For instance, the transition state corresponding to the interchange of the water monomers within the trimer lies 6.5 kcal/mol above the global minimum (at the CCSD(T) level). The first of these pathways, called the flipping pathway, involves a local minimum, the up–up (*uu*) structure, as shown in Fig. 2. The mechanism of the flipping motion is the following. First, the global and local minima are connected via a flipping transition state (a saddle point on the potential energy surface of the trimer). This transition state corresponds to the up_{Cl} structure with the free proton of one water monomer above the plane of the hydrogen-bonded ring, and the other free proton lying in the plane of the ring (up-plane and Cl since the water molecule with its external proton lying in the plane of the hydrogen-bonded ring is bonded to the chlorine atom). Thus, the flipping motion corresponds to the rotation of this water monomer about its donor hydrogen bond. Afterwards, another flipping motion, involving the p_Ou transition state, connects the *uu* structure and the global minimum *du*, the enantiomeric form of the starting *ud* minimum (plane-up and O since the water molecule with its external proton lying in the plane of the hydrogen-bonded ring is bonded to the oxygen atom). The two other pathways, called bifurcation-tunneling pathways, involve transition states with one water molecule hydrogen bonded to the other water or to the HCl monomer in a bifurcated manner. The corresponding conformation of the water monomer is obtained by rotation of this molecule around its pseudo-C_2 axis. These transition states are denoted by ub_{Cl} or bp_{Cl} depending whether the water monomer which forms the bifurcated hydrogen bond is bonded to the chlorine atom (ub_{Cl}, Fig. 3(a)) or to the oxygen atom of the other water molecule (bp_{Cl}, Fig. 3(b)). During the rotation of the bifurcated water molecule described above, a flipping of the free hydrogen of the other water molecule takes place. For the transition states and the local minimum the $O\cdots O$ and $O\cdots Cl$ distances and the $\angle ClO_AO_B$ and $\angle ClO_BO_A$ angles do not differ much from the equilibrium values. This is especially true for the flipping transition states, and suggests that the flipping motions in the trimer can be described to a good approximation by the rotation of the water monomers about their donor hydrogen bond. Note that the flipping and bifurcation-tunneling

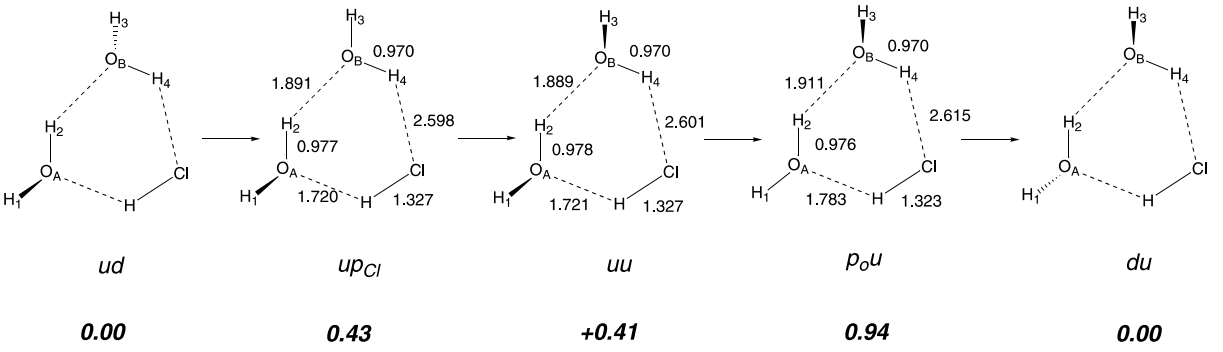

Fig. 2. Geometries of the flipping transition states on the potential energy surface of the $(H_2O)_2HCl$ trimer and a schematic representation of the flipping pathway.

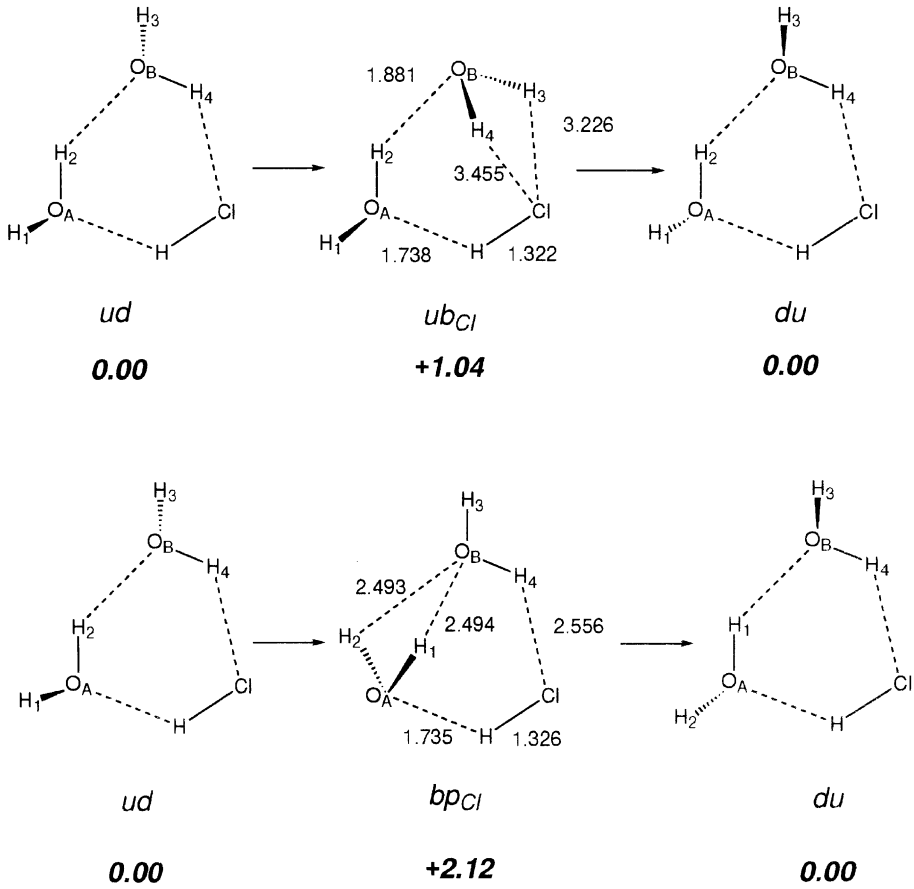

Fig. 3. Geometries of the ub_{Cl} (a) and bp_{Cl} (b) transition states on the potential energy surface of the $(H_2O)_2HCl$ trimer and a schematic representation of the corresponding bifurcation-tunneling pathways.

pathways described above are quite similar to those considered for the water trimer [54–56].

Also reported in Figs. 2, 3(a) and (b) are the energies (relative to the energy of the global minimum) of the local minimum and the saddle points on the potential energy surface of the trimer. From the total energy calculations by the CCSD(T) method it follows that the first flipping barrier in the trimer, i.e., the difference between the energies of the up_{Cl} and *ud* structures, is 0.43 kcal/mol. The height of the second flipping barrier (corresponding to the p_Ou transition state) is higher, and amounts to 0.94 kcal/mol. The local minimum *uu* is located just below the first transition state (0.41 kcal/mol). The first bifurcation-tunneling barrier, which is the difference between the energies of the ub_{Cl} and *ud* structures, is 1.04 kcal/mol, while the second transition state (the bp_{Cl} structure) is located 2.12 kcal/mol above the global minimum. One may note that the heights of the barriers separating the enantiomeric global minima are quite low, so it should be possible to observe spectroscopic transitions resulting from the tunneling between the equivalent equilibrium structures via flipping and bifurcation-tunneling pathways (see the discussion below).

3.2. Energetics of the cluster and the nature of the interactions

The interaction energies and their decomposition into pair and many-body non-additive con-

Table 1
Pair and three-body interaction energies, deformation energies, binding, and dissociation energies for various geometries of the $(H_2O)_2HCl$ cluster (energies are in kcal/mol)

Geometry	*ud*	up_{Cl}	*uu*	p_Ou	ub_{Cl}	bp_{Cl}
$E_{int}^{CCSD(T)}(2,3)$	−9.617	−9.312	−9.306	−9.323	−9.380	−8.318
$E_{int}^{CCSD(T)}(3,3)$	−2.612	−2.467	−2.498	−1.999	−2.005	−1.927
$E_{int}^{CCSD(T)}$	−12.229	−11.779	−11.804	−11.321	−11.385	−10.245
E_{def}	0.589	0.568	0.566	0.417	0.494	0.507
D_e	−11.640	−11.211	−11.238	−11.211	−10.904	−9.738
D_0	−6.890					

tributions are reported in Table 1 for the structures of the trimer described above. An inspection of this table shows that many-body cooperative effects are far from negligible. The pair interaction energy represents 80–87% of the total interaction energy of the trimer. Obviously, the structure and properties of the $(H_2O)_2HCl$ complex cannot be accurately described by assuming the pairwise additivity of the interaction potential. One may note here that the three-body effects are attractive for all the structures of the trimer considered in the present work, i.e., they represent an additional stabilizing effect.

Since the deformation energies for the global minimum and for the saddle points are quite close to each other (cf. the discussion below), the barriers separating the enantiomeric minima can, to a large extent, be recovered from the interaction energies. The corresponding values computed at the CCSD(T) level are 0.91, 0.45, 0.84, and 1.98 kcal/mol for the up_{Cl}, p_Ou, ub_{Cl}, and bp_{Cl} structures, respectively, and agree well with the results computed from the total energies, cf. Figs. 2, 3(a) and (b). (Note that the small differences between the results quoted above and those reported in the figures are only approximately consistent with the changes in the deformation energies, since the interaction energies were computed in the full basis of the trimer, while E_{def} in the bases of the respective monomers.) It follows from the pair and three-body interaction energies reported in Table 1 that the effect of the three-body forces on the barriers is dramatic. The non-additive contribution to the height of the barrier represents as much as 67% and 73% for the up_{Cl} and ub_{Cl} transition states, respectively. For the two other saddle points the three-body terms are smaller, but far from negligible. They contribute 33% and 35% to height of the barrier for the p_Ou and bp_{Cl} transition states, respectively.

In Table 1 we reported the interaction energies with respect to the monomers in the same geometries as they have in the clusters, and the binding energies with respect to the monomers in their own equilibrium structures. The latter were obtained from the interaction energies by including the monomer deformation energies. However, the experience gained for small water clusters [31] shows that the sum of the deformation energies is relatively unimportant even for the water tetramer. As shown in Table 1 this is also the case for the $(H_2O)_2HCl$ trimer: the computed binding energies D_e are rather close to the interaction energies. This is consistent with the relatively small geometry changes of the monomers upon complexation. Finally, we mention here that the dissociation energy of the complex is $D_0 = 6.89$ kcal/mol. However, care should be taken when considering this number, since the zero-point correction was computed in the harmonic approximation. Given the fact that the pathways connecting the enantiomeric minima will give rise to several strongly anharmonic vibrational modes corresponding to large-amplitude motions in the complex, the present estimate of the dissociation energy should be considered as purely qualitative.

In Table 2 we report the decomposition of the SAPT pair interaction energies into various physical contributions as defined by Eqs. (4) and (5). Before we look at the physical origins of the bonding in the $(H_2O)_2HCl$ trimer, let us first discuss the accuracy of the SAPT results. An inspection of Table 2 shows that the performance of the SAPT approach is excellent. Indeed, the

Table 2
Components of the pair and three-body interaction energies for various geometries of the $(H_2O)_2HCl$ cluster (energies are in kcal/mol)

Geometry	*ud*	up_{Cl}	*uu*	$p_O u$	ub_{Cl}	bp_{Cl}
$E^{(1)}_{elst}$	−27.235	−25.523	−25.801	−22.273	−25.228	−22.131
$E^{(2)}_{ind}$	−16.199	−14.511	−15.279	−11.807	−14.385	−12.989
$E^{(2)}_{disp}$	−10.103	−9.762	−9.808	−8.703	−9.145	−8.714
E_{attr}	−53.537	−49.796	−50.888	−42.783	−48.758	−43.834
E_{exch}	43.752	40.284	41.421	33.166	39.298	35.474
$E^{SAPT}_{int}(2,3)$	−9.786	−9.512	−9.467	−9.617	−9.460	−8.360
$E^{CCSD(T)}_{int}(2,3)$	−9.617	−9.312	−9.306	−9.323	−9.380	−8.318
$E^{CCSD(T)}_{int}(3,3)$	−2.612	−2.467	−2.498	−1.999	−2.005	−1.927
$E^{CCSD(T)}_{int}$	−12.229	−11.779	−11.804	−11.321	−11.385	−10.245

comparison of the SAPT and CCSD(T) pair interaction energies shows that the deviations between the two sets of results are of the order of 1–2%, the largest being 3%. This level of agreement between the results from highly correlated supermolecule and perturbative calculations suggests that the SAPT method is a good tool to describe pair interactions in the clusters of water and HCl.

Let us discuss the most important contributions responsible for the bonding in the $(H_2O)_2HCl$ trimer. As the results reported in Table 2 show, for all geometries considered in the present paper the electrostatic energy is by far the largest contribution to the interaction energy. This could be expected since the hydrogen bond is directional, and the structure of hydrogen-bonded complexes is largely determined by the electrostatic interactions. However, other contributions are far from negligible. For instance, the pair induction and dispersion energies are of the same order of magnitude as the total interaction energy, while the pairwise additive exchange term is more than twice the total interaction energy (in absolute value). Hence, the pairwise additive interaction energy is not dominated by a single component, but rather results from a partial cancellation of large attractive and repulsive contributions. This conclusion is valid for all the geometries considered in Table 2. In fact, a closer analysis of the results suggests that the global minimum corresponds to a structure with the largest attractive contributions (the sum $E^{(1)}_{elst} + E^{(2)}_{ind} + E^{(2)}_{disp}$ denoted in the table by E_{attr}), and the highest exchange-repulsion term. The local minimum and the transition states, in turn, show smaller attractive terms and lower repulsion (with respect to their values for the global minimum). One may note here that the picture of the intermolecular interactions in the $(H_2O)_2HCl$ trimer is similar to that reported in Ref. [40] for the water trimer. We wish to end this section by saying that the three-body interactions in the $(H_2O)_2HCl$ trimer are mainly governed by the induction and exchange-deformation terms. These two contributions can be easily calculated at the Hartree–Fock level. Other terms are small. See Ref. [41] for a more detailed discussion of the nature and importance of three-body forces in $(H_2O)_2HCl$. Thus, a full potential energy surface for this trimer could be rather easily obtained, despite the large number of the degrees of freedom.

3.3. Molecular properties

In Table 3 we present the components of the dipole moment vector of the trimer with respect to the principal axes of the complex (μ_a, μ_b, and μ_c), computed at various levels of the theory. For comparison, also reported are the components of the dipole moment for the water and HCl monomers. An inspection of this table shows that the dipole moment is not very sensitive to the level of the electron correlation included in the calculations. Indeed, the total dipole moment at the MP2 level is only 2.5% lower than its Hartree–Fock value. The inclusion of the CCSD(T) correlation results in a further decrease by 1.7%. Similar trends are observed for the components of the dipole moment vector.

Table 3
The dipole moments of HCl, H_2O and of $(H_2O)_2HCl$ (in D) calculated at the aug-cc-pVDZ/MP2 geometry: electron correlation effects and dipole moment enhancement

	HF	MP2	MP3	MP4	CCSD(T)
HCl					
μ	1.241	1.171	1.158	1.133	1.132
H_2O					
μ	1.999	1.867	1.885	1.839	1.847
$(H_2O)_2HCl$					
μ_T	2.481	2.422	2.409	2.382	2.381
μ_a	2.393	2.349	2.329	2.306	2.304
μ_b	−0.636	−0.574	−0.594	−0.579	−0.585
μ_c	0.155	0.150	0.149	0.147	0.148
μ_S[a]	1.705	1.595	1.606	1.567	1.573
$\Delta\mu$[b]	1.112	1.141	1.130	1.131	1.129
$\angle(\vec{\mu}_T, \vec{\mu}_S)$	22.3	23.0	23.3	23.4	23.5

[a] Dipole moment calculated by vector addition of the three monomer dipoles.
[b] The dipole moment enhancement, which is the magnitude of the vectorial quantity $\Delta\vec{\mu} = \vec{\mu}_T - \vec{\mu}_S$.

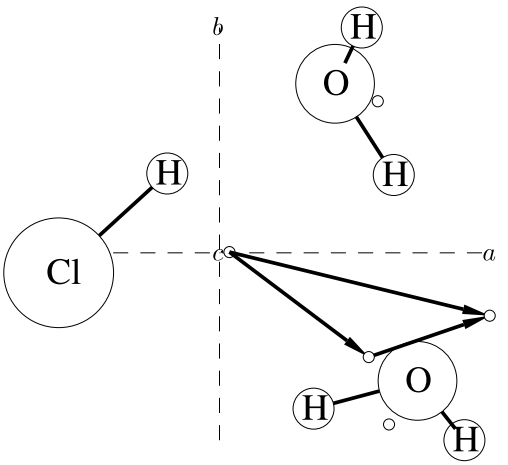

Fig. 4. The orientation of the total electric dipole moment, $\vec{\mu}_T$, the dipole moment obtained by vector summation of the dipole moments of the isolated monomers, $\vec{\mu}_S$, and the resulting dipole moment enhancement, $\Delta\vec{\mu} = \vec{\mu}_T - \vec{\mu}_S$. The monomer dipole moments are also indicated to the same scale.

One may note that the dipole moment of the complex is strongly enhanced compared to the dipole moment resulting from the addition of the three dipole moment vectors of the respective monomers. The dipole moment enhancement represents as much as 47% of the dipole moment of the complex. The orientations of the pertinent dipole moment vectors are shown in Fig. 4 in which it can be seen that the additional polarization $\Delta\mu$ is in the general direction between the HCl and the $(H_2O)_2$ subunits. It is near-perpendicular to the $OH\cdots O$ hydrogen bond, but is reasonably consistent with the direction of the $ClH\cdots O$ bond. Although it is still premature to identify the contributions to $\Delta\mu$ we note that its magnitude is considerable and is well in excess of values of the dipole enhancement measured for dimers, e.g. 0.80 D for $HCN\cdots HF$ [57], 0.68 D for $H_2O\cdots HF$ [58,59], or 0.67 D for benzene$\cdots$HF [60]. Given the importance of the electrostatic energy for the stabilization of the trimer, one can guess that the mechanism leading to such a large dipole moment enhancement is governed by the polarization of the HCl molecule by the electric charge distributions on the two water monomers [61].

In Table 4 we present the basis-set dependence of the dipole moment and its components computed at the MP2 level, as well as the comparison between the theory and experiment. An inspection of this table shows that the basis-set dependence is not very pronounced, the differences between the results computed in the aug-cc-pVDZ and aug-cc-pVTZ bases being of the order of a few percent. Helgaker and collaborators [62] suggested that the basis-set limit of a molecular property P can be obtained from two calculations carried out with two correlation consistent basis sets. Specifically, if P_x denotes the value of the property computed with the aug-cc-pVxZ basis, then a good approximation to the basis-set limit can be obtained from the following extrapolation formula:

Table 4
The dipole moment of $(H_2O)_2HCl$ (in D) calculated at the aug-cc-pVDZ/MP2 geometry: basis-set dependence and comparison with experiment

	aug-cc-pVDZ	aug-cc-PVTZ	Extrapolated	Best estimate	Experiment[a]
μ_T	2.422	2.375	2.355	2.314	2.328(3)
μ_a	2.349	2.295	2.272	2.227	2.232(3)
μ_b	−0.574	−0.595	−0.604	−0.615	0.662(2)
μ_c	0.150	0.151	0.151	0.149	0.0[b]

[a] Experimental values are taken from Ref. [24].
[b] Assumed value.

$$P_{\text{extr}} = \frac{x^3 P_x - y^3 P_y}{x^3 - y^3}, \tag{6}$$

where usually $y = x + 1$. The extrapolations of the total dipole moment and its components are reported in Table 4. The extrapolated values are lower than those computed in the aug-cc-pVTZ basis by atmost 1.5%. To get the best theoretical estimate of the dipole moment and its components we employed the following scheme. The basis-set limit at the MP2 level was obtained from Eq. (6), while the correlation contribution beyond the MP2 level was obtained as the difference between the CCSD(T) and MP2 results computed in the aug-cc-pVDZ basis. As shown in Table 4 the best estimates agree very well with the experimental data [24]. The only exception is the b component of the dipole moment. However, this component is rather small, and the disagreement of the order of 7% is not dramatic. It can partly be attributed to the ground-state averaging effects inherent in the experimental value [24].

In Table 5 we report the nuclear quadrupole coupling constants for the chlorine nucleus in the $(H_2O)_2HCl$ cluster computed at the MP2 level in two basis sets of different quality. An inspection of the results shows that the components of the nuclear quadrupole coupling tensor are not very sensitive to the quality of the basis set used in the calculations. The variations of χ_{ii}, $i = x,y,z$, with the basis do not represent more than 7%. Similar trends are observed for the nuclear quadrupole asymmetry parameter η. The extrapolated values using Eq. (6) are in good agreement with the experiment, the deviation being of the order of ≈4%. This 4% difference can be attributed to the sum of the correlation effects beyond the MP2 level, and to possible ground-state average effects inherent in the experimental values.

Table 5
Nuclear quadrupole coupling constants (in MHz) for the chlorine nucleus in the $(H_2O)_2HCl$ cluster calculated at the aug-cc-pVDZ/MP2 geometry

	aug-cc-pVDZ	aug-cc-pVTZ	Extrapolated	Experiment[a]
χ_{zz}	−43.15	−46.16	−47.43	−49.4(5)
χ_{xx}	19.94	21.23	21.77	22.8(5)
χ_{yy}	23.21	24.93	25.65	26.60(15)
η[b]	0.076	0.080	0.082	0.077

[a] Experimental values are taken from Ref. [23].
[b] The nuclear quadrupole asymmetry parameter, $\eta = (\chi_{xx} - \chi_{yy})/\chi_{zz}$.

3.4. Vibration–rotation–tunneling motions

Thus far we have discussed the structure, energetics, and the properties of the complex. Having determined the possible tunneling pathways connecting the enantiomeric minima, we can now turn to the classification of the vibration–rotation–tunneling (VRT) states of the complex. The largest possible permutation-inversion (PI) group of the complex is G_{16}. This group is obtained by considering the permutations of the protons within the two identical monomers, the permutation of the water monomers themselves, and the space-fixed inversion. Since the permutation of the two water monomers corresponds to an unfeasible operation, the PI group is reduced to $G_8 = \{E, E^*, (12), (34), (12)(34), (12)^*, (34)^*, (12)(34)^*\}$ [63,64]. Thus, the VRT states of the complex can be classified according to the irreducible representations (irreps) of this group. The G_8 group can conveniently be represented as a direct product $G_8 = \{E, E^*\} \otimes \{E, (12), (34), (12)(34)\}$, so the classification of the VRT states can be obtained from the correlation between the states classified under $G_2 = \{E, E^*\}$ and G_8. One may note that the flipping motions in the complex are governed by the PI operation E^*, while the tunneling motions corresponding to the bifurcation-tunneling pathways are governed by the PI operations $(12)^*$ and $(34)^*$. Since the flipping barriers separating the equivalent minima are low, one can expect that the VRT levels can, in the first approximation, be classified according to the irreps of G_2. The corresponding energy levels will be denoted by E_{A^+} and E_{A^-}. The correlation between the irreps of G_2 and G_8 shows that the states $A^{\pm}$ are split into quartets with symmetry labels $A^{\pm}_{1,2}$ and $B^{\pm}_{1,2}$. Thus, the bifurcation-tunneling motions introduce the splitting of the flipping tunneling states into quartets. Since the barriers corresponding to the bifurcation-tunneling motions are larger, one may expect that the splitting into quartets will be much smaller than the splitting

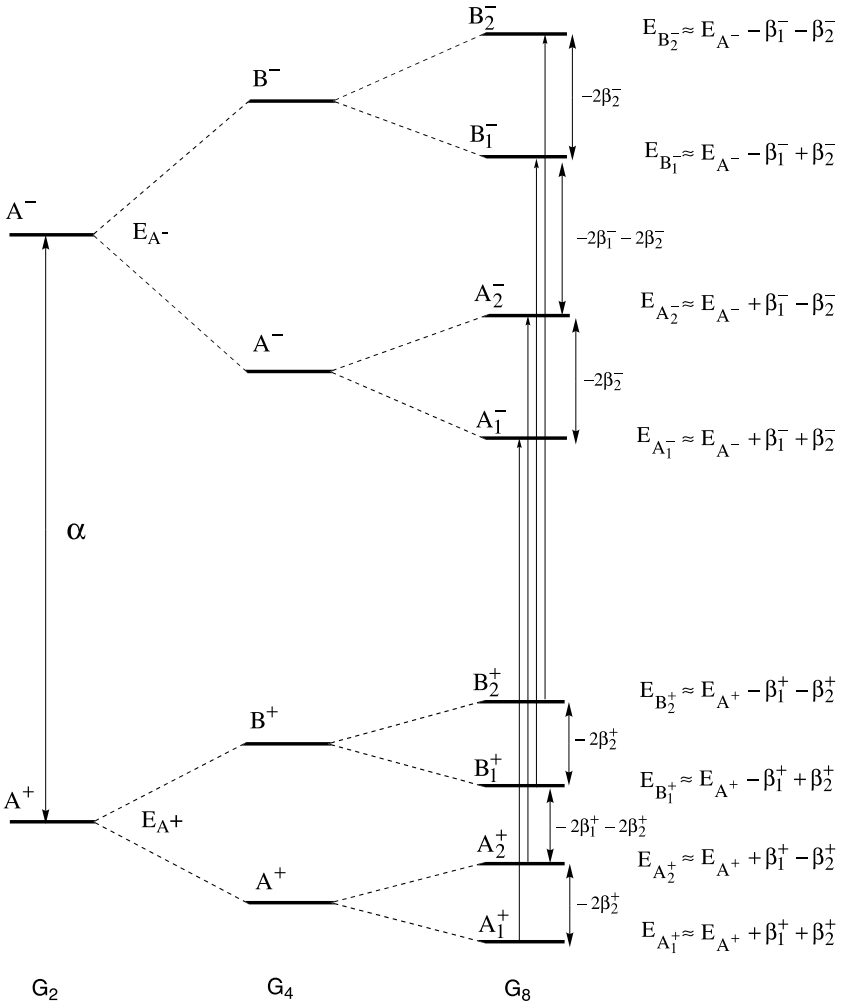

Fig. 5. Schematic representation of the energy levels for the non-rotating ($J = 0$) $(H_2O)_2HCl$ and $(HOD\cdots OH_2)\cdots HCl$ clusters according to the groups G_8 and G_4, respectively.

corresponding to the flipping motions. The schematic representation of the energy levels for the non-rotating $(H_2O)_2HCl$ trimer are presented in Fig. 5.

To obtain an approximate location of the energy, we will use the following representation of the total Hamiltonian for the nuclear motion:

$$H = H_{\text{int}} + H_{\text{asym}} + H_{\text{Cor}}, \tag{7}$$

where the consecutive terms on the right-hand side denote Hamiltonians describing the internal motions, the external rotational part given by the asymmetric top Hamiltonian, and the Coriolis coupling term. We follow Van der Avoird and coworkers [65] and split the internal Hamiltonian into parts exclusively describing the flipping and bifurcation-tunneling motions in the complex:

$$H_{\text{int}} = H_{\text{flip}} + H_{\text{bif}} + V. \tag{8}$$

Here, H_{flip} and H_{bif} are the Hamiltonians describing the flipping and bifurcation-tunneling motions, respectively, and V is the intermolecular potential. The Hamiltonians H_{flip} and H_{bif} depend exclusively on those coordinates of the complex that define

these motions, i.e., on the set of two torsional angles (χ_1, χ_2) for the flipping motion, and on two bifurcation-tunneling coordinates (t_1, t_2) for the bifurcation-tunneling motions. For the purpose of our discussion their precise definition is not necessary. It is given in Ref. [66], where we report more quantitative results for the potential energy surface and VRT states for the flipping motions in the complex. In the following we will consider explicitly the non-rotating $J = 0$ case, so the two last terms on the right-hand side of Eq. (7) can be neglected. We will also assume that the intermolecular potential does not depend on the tunneling coordinates (t_1, t_2), and that the eigenvalues and eigenfunctions of the Hamiltonian describing the flipping motion, $H_{\text{flip}} + V$, are known. The corresponding wave functions $\Psi_{A^{\pm}}$ are adapted to the G_2 group. Then, the eigenvalues of H_{int} can be found by computing the expectation value of this Hamiltonian with wave functions obtained from $\{\Psi_{A^+}, \Psi_{A^-}\}$ by symmetry adaptation to G_8. The corresponding wave functions are obtained by applying Wigner's symmetry projection operators of the group $G_4 = \{E, (12), (34), (12)(34)\}$ on Ψ_{A^+} and Ψ_{A^-}, and are given by:

$$\Psi_{A^+_{1,2}} = \tfrac{1}{2}(E + (12) \pm (34) \pm (12)(34))\Psi_{A^+}, \tag{9}$$

$$\Psi_{B^+_{1,2}} = \tfrac{1}{2}(E - (12) \pm (34) \mp (12)(34))\Psi_{A^+}, \tag{10}$$

$$\Psi_{A^-_{1,2}} = \tfrac{1}{2}(E + (12) \pm (34) \pm (12)(34))\Psi_{A^-}, \tag{11}$$

$$\Psi_{B^-_{1,2}} = \tfrac{1}{2}(E - (12) \pm (34) \mp (12)(34))\Psi_{A^-}. \tag{12}$$

The upper and lower signs appearing in Eqs. (9)–(12) correspond to the irrep labels indexed by 1 and 2, respectively. Note that the wave functions $\Psi_{A^{\pm}}$ have a definite parity with respect to the space-fixed inversion E^*, so the permutation operations in Eqs. (9)–(12) can be replaced by the PI operations multiplied by the parity of the state. Since we want to give a qualitative description of the energy levels, we can leave from Eqs. (9)–(12) those PI operations that are not involved in the bifurcation-tunneling pathway, i.e. we can approximately omit in Eqs. (9)–(12) the operations E and (12)(34). One can expect that the corresponding matrix elements of the Hamiltonian, although non-zero, will be much smaller than the matrix elements involving the PI operations directly involved in the tunneling motion. This leads to the energy levels diagram presented in Fig. 5. The quantity α represents the splitting of the levels exclusively due to the flipping motions. The parameters $\beta^{\pm}_{1,2}$, which define the splitting of the tunneling flipping states into quartets, are given by the following matrix elements:

$$\beta^{\pm}_{1,2} = \langle E^* \Psi_{A^{\pm}} | H_{\text{bif}} \pi_{1,2} \Psi_{A^{\pm}} \rangle, \qquad \pi_1 = (12), \quad \pi_2 = (34). \tag{13}$$

Obviously, the ground state of the complex must be described by the totally symmetric (nodeless) wave function, so it is of A_1^+ symmetry. This suggests that both β_1^+ and β_2^+ are negative. It is, nevertheless, very difficult to estimate the magnitude of the parameters $E_{A^{\pm}}$ and $\beta^{\pm}_{1,2}$ without a prior knowledge of the potential energy surface of the cluster. The results of our dynamical calculations [66] show that the splitting due to the flipping motions, i.e. the parameter α is rather large ≈ 19 cm^{-1}. The experience gained for the water clusters suggests that the splitting of the flipping levels into quartets is much smaller, of the order of a several hundred MHz [65].

The allowed dipole transitions can be determined by satisfying [63]:

$$\Gamma_1 \otimes \Gamma_2 \supset \Gamma^* = A_1^-, \tag{14}$$

where Γ_1 and Γ_2 are the irreps corresponding to two VRT states, and Γ^* is the antisymmetric irrep of G_8. This leads to the following dipole selection rules:

$$A^+_{1,2} \leftrightarrow A^-_{1,2} \qquad B^+_{1,2} \leftrightarrow B^-_{1,2}. \tag{15}$$

Thermal relaxation between states of the same $A_{1,2}$ or $B_{1,2}$ symmetry will occur independently of the parity, so at very low temperatures the upper quartet states will be much less populated.

Finally, the intensity pattern that should be observed in the microwave experiments can be obtained by considering the spin-statistical weights. These have been obtained by generating the representation spanned by all possible proton spin functions:

$$\Gamma_{\text{spin}}^{\text{tot}} = 18A_1 \oplus 6A_2 \oplus 6B_1 \oplus 2B_2 \tag{16}$$

and by requiring that (Ref. [63], p. 231)

$$\Gamma_{\text{spin}} \otimes \Gamma_{\text{VRT}} \supset \Gamma_{\text{int}} \equiv B_2, \tag{17}$$

where Γ_{spin} denotes one of the irreps entering the decomposition of $\Gamma_{\text{spin}}^{\text{tot}}$, Eq. (16). (Note that in this case we can consider the pure permutation group G_4, since the inversion operation does not affect the spin functions.) The equality (17) simply means that the product of the internal wave function classified according to the Γ_{VRT} irrep multiplied by a spin function is a fermionic wave function. The resulting spin-statistical weights are reported in Table 6. The weights reported in this table show that the expected intensity pattern is 9:3:3:1.

The qualitative picture of the tunneling dynamics presented above, and the large values of the computed *a* and *b* components of the dipole moment (cf. Section 3.3) suggest that the lowest lying vibrational states of $(H_2O)_2HCl$ will arise from the VRT motions of the two water subunits in the cluster, and are predicted to be of B_2^+, B_1^+, A_2^+, and A_1^+ symmetry with the spin-statistical weights of 18:6:6:2, respectively. Thus, the rotational spectrum should consist of transitions allowed by the *a* and *b* dipole moment components, which are further split into quartets belonging to the four low-lying VRT states.

It is worth noting that the PI group for various isotopomers of $(H_2O)_2HCl$ will not necessarily be G_8. For instance, for the $(HOD\cdots OH_2)\cdots HCl$ isotopomer the PI group will be $G_4 = \{E, E^*\} \otimes \{E, (34)\}$, since the proton H_2 is substituted with a deuteron D. In this case, the flipping tunneling states will split into doublets of $A^{\pm}$ and $B^{\pm}$ symmetry (cf. Fig. 5).

To end this section we wish to say that the qualitative picture of the spectroscopic features of the $(H_2O)_2HCl$ trimer is a very good agreement with the microwave measurements [23]. The rotational spectra of $(H_2O)_2HCl$ show four states that can be assigned to B_2^+, B_1^+, A_2^+, and A_1^+ symmetries, in agreement with the G_8 picture discussed above. Furthermore, the spectrum of the $(HOD\cdots OH_2)\cdots HCl$ isotopomer shows splittings into A^+ and B^+ doublets, again in agreement with our predictions based on the G_4 PI group. The most intense transitions observed in the experimental spectrum are of *a*-type, in agreement with the large value of the *a* component of the dipole moment. No *c*-type transitions could be observed. This is again confirmed by the very small value of μ_c. The relative intensities observed in the experiment are 4:2:2:1, while our theoretical prediction based on the G_8 picture is 9:3:3:1. We believe that the source of this small disagreement is in the specific non-equilibrium properties of the supersonic expansion.

Table 6
Spin-statistical weights for the $(H_2O)_2HCl$ cluster

Γ_{VRT}	Γ_{spin}	Γ_{int}	Weight
A_1	$2B_2$	B_2	2
A_2	$2B_1$	B_2	6
B_1	$10A_2$	B_2	6
B_2	$18A_1$	B_2	18

4. Conclusions

In this paper we reported ab initio calculations of the structure, energetics, and properties of the $(H_2O)_2HCl$ complex, of the low-energy tunneling pathways and of the corresponding rearrangement mechanisms. The spectroscopic consequences of our structural and dynamical study were also investigated. The results of this paper can be summarized as follows:

1. The global minimum on the potential energy surface of the $(H_2O)_2HCl$ trimer corresponds to a cyclic triangular hydrogen-bonded structure with both HCl and the two water monomers acting simultaneously as proton donors and acceptors. The heavy atoms form a slightly deformed equilateral triangle. The hydrogen atoms forming hydrogen bonds lie almost perfectly in the plane of the heavy atoms, while the external protons are strongly distorted from the hydrogen-bonded ring. This structure has no spatial symmetry, but there are two equivalent minima corresponding to the *ud* and *du* enantiomeric structures.

2. The two equivalent minima on the potential energy surface are interconnected by three low-energy tunneling pathways corresponding to the

hydrogen-bond network rearrangement processes. The lowest energy rearrangement pathway corresponds to the flipping of one of the free hydrogen atoms across the plane of the hydrogen-bonded ring. Two other mechanisms involve transition states with one water molecule hydrogen bonded to the other water or HCl monomer in a bifurcated manner. The heights of the barriers corresponding to these transition states are quite low, so it should be possible to observe spectroscopic transitions resulting from the tunneling between the equivalent equilibrium structures via these pathways.

3. Supermolecule calculations of the pair and three-body interaction energies show that the structure and properties of the $(H_2O)_2HCl$ complex cannot be accurately described by assuming the pairwise additivity of the interaction potential, the three-body terms representing as much as 13–20% of the total interaction energy of the trimer. The non-additive contribution to the heights of the barriers is even larger. For some transition states it may represent almost 75% of the total barrier height. The computed binding energies are rather close to the interaction energies, in agreement with the relatively small geometry changes of the monomers upon complexation.

4. An analysis of the nature of the interaction in the complex by SAPT revealed that the cluster is mainly bound by the electrostatic and induction forces. However, the dispersion energy also represents an important stabilizing contribution. The comparison of the perturbative SAPT and supermolecule CCSD(T) results shows that the performance of the SAPT method is excellent: the deviations of the SAPT results from the corresponding CCSD(T) values are of the order of 1–2%.

5. The $(H_2O)_2HCl$ cluster has a large dipole moment, with the largest components along the *a* and *b* inertial axes. The dipole moment of the complex is strongly enhanced compared to the dipole moment resulting from the addition of the three dipole moment vectors of the respective monomers. This shows that there is a considerable flow of the charge within the complex, and suggests that the mechanism leading to such a large dipole moment enhancement is governed by the polarization of the HCl molecule by the electric charge distributions on the water monomers.

6. From the low-energy pathways connecting the two enantiomeric minima it follows that the VRT states of the complex can be classified according to the irreps of the G_8 group. It is shown, by the use of a model Hamiltonian and by group theory with the G_2 group for the flipping motion and the full G_8 group if the rotating pathway is allowed, that the splittings can be derived algebraically. It is further shown that the rotating motion splits every flipping tunneling state into quartets. The corresponding intensity pattern that is predicted for rotational transitions observed in the microwave experiments is 9:3:3:1.

7. The large values of the *a* and *b* components of the dipole moment vector and the picture of the tunneling dynamics based on the G_8 PI group suggest that the rotational spectrum will consist of transitions allowed by the *a* and *b* dipole moment components, which are split into quartets belonging to the four low-lying VRT substates of A_1^+, A_2^+, B_1^+, and B_2^+ symmetry.

8. Our theoretical predictions concerning the structure, the values of the electric dipole moment components, and of the nuclear quadrupole coupling constants are in a very good agreement with the data obtained from the microwave measurements [23,24]. Also the qualitative picture of the spectra predicted in the present paper fully explains the observed pattern of lines in the rotational spectra of the $(H_2O)_2HCl$ trimer and its partly deuterated isotopomers.

Of course, a quantitative comparison with the present and future spectroscopic experiments requires the knowledge of the potential energy surface for the trimer, and of the bound states corresponding to various rotation–vibration tunneling states of the complex. A step in this direction has been done in Ref. [66], where we report a SAPT potential for the flipping motions in the trimer, and predict the energy levels, tunneling splittings, and line strengths of the far-infrared transitions.

Acknowledgements

We would like to thank Bogumil Jeziorski for reading the manuscript and for useful comments.

The calculations were performed in Grenoble, in Warsaw, and at the Centre IDRIS (Project 991219 and 001219) of CNRS (Centre National de la Recherche Scientifique, Orsay, France). CNRS, the University Joseph Fourier of Grenoble, and the University of Warsaw are acknowledged for providing the computer facilities.

References

[1] H. Haberland (Ed.), Clusters of Atoms and Molecules, vol. I and II, Springer, Berlin, 1995.
[2] D.D. Nelson, K.R. Leopold, W. Klemperer, in: E.R. Bernstein (Ed.), Atomic and Molecular Clusters, Elsevier, Amsterdam, 1990.
[3] B. Jeziorski, R. Moszynski, K. Szalewicz, Chem. Rev. 94 (1994) 1887.
[4] G. Chalasinski, M.M. Szczesniak, S.M. Cybulski, in: Z.B. Maksic, W.J. Orville-Thomas (Eds.), Modern Modelling of the Chemical Bond, Theoretical and Computational Chemistry, vol. 6, Elsevier, Amsterdam, 1997.
[5] J.E. Del Bene, M.J.T. Jordan, Int. Rev. Phys. Chem. 18 (1999) 119.
[6] J.E. Del Bene, M.J.T. Jordan, J. Am. Chem. Soc. 122 (2000) 4794.
[7] J.E. Del Bene, S.A. Perera, R.J. Bartlett, J. Am. Chem. Soc. 122 (2000) 3561.
[8] D.R. Handon, A.R. Ravishankara, J. Phys. Chem. 96 (1992) 2682.
[9] L.T. Chu, M.T. Leu, L.F. Keyser, J. Phys. Chem. 97 (1993) 12798.
[10] M.R.S. McCoustra, A.B. Horn, Chem. Soc. Rev. 23 (1994) 195.
[11] L. Wang, D.C. Clary, J. Chem. Phys. 104 (1996) 5663.
[12] K. Ando, T.J. Hynes, J. Mol. Liq. 64 (1995) 25.
[13] D.A. Estrin, J. Kohonoff, D.H. Laaria, R.O. Weht, Chem. Phys. Lett. 280 (1997) 280.
[14] Z. Latajka, S. Scheiner, J. Chem. Phys. 87 (1987) 5928.
[15] C. Chipot, L.G. Gorb, J.-L. Rivail, J. Phys. Chem. 98 (1994) 1601.
[16] C. Lee, C. Sosa, M. Planas, J.J. Novoa, J. Chem. Phys. 104 (1996) 7081.
[17] S. Re, Y. Osamura, Y. Suzuki, H.F. Schaefer III, J. Chem. Phys. 109 (1998) 973.
[18] A. Smith, M.A. Vincent, I.H. Hillier, J. Phys. Chem. A 103 (1999) 1132.
[19] D.E. Bacelo, R.C. Binning Jr., Y. Ishikawa, J. Phys. Chem. A 103 (1999) 4631.
[20] M.J. Packer, D.C. Clary, J. Phys. Chem. 99 (1995) 14323.
[21] A.C. Legon, L.C. Willoughby, Chem. Phys. Lett. 95 (1983) 449.
[22] Z. Kisiel, B.A. Pietrewicz, P.W. Fowler, A.C. Legon, E. Steiner, J. Phys. Chem. A 104 (2000) 6970.
[23] Z. Kisiel, E. Białkowska-Jaworska, L. Pszczółkowski, A. Milet, C. Struniewicz, R. Moszynski, J. Sadlej, J. Chem. Phys. 112 (2000) 5767.
[24] Z. Kisiel, J. Kosarzewski, B.A. Pietrewicz, L. Pszczółkowski, Chem. Phys. Lett. 325 (2000) 523.
[25] C. Struniewicz, A. Milet, J. Sadlej, R. Moszynski, Int. J. Quant. Chem., Special issue devoted to the memory of Prof. S. Kwiatkowski, 2001, in press.
[26] A. Milet, C. Struniewicz, R. Moszynski, P.E.S. Wormer, J. Chem. Phys. 115 (2001) 349.
[27] M.J. Frisch, G.W. Trucks, H.B. Schlegel, G.E. Scuseria, M.A. Robb, J.R. Cheeseman, V.G. Zakrzewski, J.A. Montgomery Jr., R.E. Stratmann, J.C. Burant, S. Dapprich, J.M. Millam, A.D. Daniels, K.N. Kudin, M.C. Strain, O. Farkas, J. Tomasi, V. Barone, M. Cossi, R. Cammi, B. Mennucci, C. Pomelli, C. Adamo, S. Clifford, J. Ochterski, G.A. Petersson, P.Y. Ayala, Q. Cui, K. Morokuma, D.K. Malick, A.D. Rabuck, K. Raghavachari, J.B. Foresman, J. Cioslowski, J.V. Ortiz, B.B. Stefanov, G. Liu, A. Liashenko, P. Piskorz, I. Komaromi, R. Gomperts, R.L. Martin, D.J. Fox, T. Keith, M.A. Al-Laham, C.Y. Peng, A. Nanayakkara, C. Gonzalez, M. Challacombe, P.M.W. Gill, B. Johnson, W. Chen, M.W. Wong, J.L. Andres, C. Gonzalez, M. Head-Gordon, E.S. Replogle, J.A. Pople, Gaussian, Pittsburgh PA, 1998.
[28] T.H. Dunning Jr., J. Chem. Phys. 90 (1989) 1007.
[29] R.A. Kendall, T.H. Dunning Jr., R.J. Harrison, J. Chem. Phys. 96 (1992) 6769.
[30] S.S. Xantheas, T.H. Dunning, J. Chem. Phys. 99 (1993) 8774.
[31] S.S. Xantheas, J. Chem. Phys. 100 (1994) 7523.
[32] S.S. Xantheas, L.X. Dang, J. Phys. Chem. 100 (1996) 3989.
[33] S.F. Boys, F. Bernardi, Mol. Phys. 19 (1970) 553.
[34] G. Zirz, R. Ahlrichs, J. Chem. Phys. 85 (1981) 4989.
[35] R. Moszynski, P.E.S. Wormer, B. Jeziorski, A. van der Avoird, J. Chem. Phys. 103 (1995) 8058.
[36] R. Moszynski, P.E.S. Wormer, B. Jeziorski, A. van der Avoird, J. Chem. Phys. 107 (1997) E672.
[37] V. Lotrich, K. Szalewicz, J. Chem. Phys. 106 (1997) 9668.
[38] R. Moszynski, P.E.S. Wormer, T.G.A. Heijmen, A. van der Avoird, J. Chem. Phys. 108 (1998) 579.
[39] N. Turki, A. Milet, A. Rahmouni, O. Ouamerali, R. Moszynski, E. Kochanski, P.E.S. Wormer, J. Chem. Phys. 109 (1998) 7157.
[40] A. Milet, R. Moszynski, P.E.S. Wormer, A. van der Avoird, J. Phys. Chem. A 103 (1999) 6811.
[41] A. Milet, C. Struniewicz, P.E.S. Wormer, R. Moszynski, Theor. Chem. Acc. 104 (2000) 195.
[42] K. Szalewicz, B. Jeziorski, Mol. Phys. 38 (1979) 191.
[43] R. Moszynski, B. Jeziorski, A. Ratkiewicz, S. Rybak, J. Chem. Phys. 99 (1993) 8856.
[44] R. Moszynski, B. Jeziorski, K. Szalewicz, J. Chem. Phys. 100 (1994) 1312.
[45] R. Moszynski, B. Jeziorski, S. Rybak, K. Szalewicz, H.L. Williams, J. Chem. Phys. 100 (1994) 5080.
[46] R. Moszynski, S.M. Cybulski, G. Chalasinski, J. Chem. Phys. 100 (1994) 4998.

[47] S. Rybak, B. Jeziorski, K. Szalewicz, J. Chem. Phys. 95 (1991) 6576.
[48] G. Chalasinski, B. Jeziorski, Theor. Chim. Acta 46 (1977) 277.
[49] M. Jeziorska, B. Jeziorski, J. Cizek, Int. J. Quant. Chem. 32 (1987) 149.
[50] R. Moszynski, T.G.A. Heijmen, B. Jeziorski, Mol. Phys. 88 (1996) 741.
[51] R.J. Bemish, L. Oudejans, R.E. Miller, R. Moszynski, T.G.A. Heijmen, P.E.S. Wormer, A. van der Avoird, J. Chem. Phys. 109 (1998) 8968.
[52] B. Jeziorski, R. Moszynski, A. Ratkiewicz, S. Rybak, K. Szalewicz, H.L. Williams, SAPT: a program for many-body symmetry-adapted perturbation theory calculations of intermolecular interactions, in: E. Clementi (Ed.), Methods and Techniques in Computational Chemistry: METECC-94, vol. B: Medium Size Systems, STEF, Cagliari, 1993, p. 79.
[53] M. Schütz, T. Bürgi, S. Leutwyler, H.B. Bürgi, J. Chem. Phys. 99 (1993) 5228.
[54] D.J. Wales, J. Am. Chem. Soc. 115 (1993) 11180.
[55] M. Schütz, T. Bürgi, S. Leutwyler, J. Chem. Phys. 99 (1993) 5228.
[56] K. Liu, J.G. Loeser, M.J. Elrod, B.C. Host, J.A. Rzepiela, R.J. Saykally, J. Am. Chem. Soc. 116 (1994) 3507.
[57] A.C. Legon, D.J. Millen, S.C. Rogers, Proc. R. Soc. London A 370 (1980) 2130.
[58] Z. Kisiel, A.C. Legon, D.J. Millen, J. Chem. Phys. 78 (1983) 2910.
[59] Z. Kisiel, A.C. Legon, D.J. Millen, Proc. R. Soc. London A 381 (1982) 419.
[60] F.A. Baiocchi, J.H. Williams, W. Klemperer, J. Am. Chem. Soc. 87 (1983) 2079.
[61] T.G.A. Heijmen, R. Moszynski, P.E.S. Wormer, A. van der Avoird, Mol. Phys. 89 (1996) 81.
[62] T. Helgaker, K. Bak, A. Halkier, P. Jørgensen, J. Olsen, W. Klopper, J. Phys. B 32 (1999) R103.
[63] P.R. Bunker, Molecular Symmetry and Spectroscopy, Academic Press, New York, 1979.
[64] A. van der Avoird, P.E.S. Wormer, R. Moszynski, Chem. Rev. 94 (1994) 1931.
[65] A. van der Avoird, E.H.T. Olthof, P.E.S. Wormer, J. Chem. Phys. 105 (1996) 8034.
[66] C. Struniewicz, T. Korona, R. Moszynski, A. Milet, Chem. Phys. Lett. 343 (2001) 588.